Understanding Moisture Variations in Madden-Julian Oscillation in NCAR CAM5.3

Mengmiao Yang

Institute of Geography, Key Laboratory for Humid Subtropical Eco-Geographical Processes of the Ministry of Education, Fujian Normal University

Guyu Cao

Shenzhen Capital Group, Shenzhen, China

School of Economics and Management, Tsinghua University

Guang J. Zhang

Scripps Institution of Oceanography, La Jolla, California

Yong Wang

Department of Atmospheric and Oceanic Sciences, Fudan University

For submission to J. Climate

Revised on April 17, 2025

Corresponding author: Guang J. Zhang, Scripps Institution of Oceanography, La Jolla, CA 92093. Email: gzhang@ucsd.edu

Abstract

Previous observational and modeling studies have suggested that moisture plays a dominant role in Madden-Julian Oscillation (MJO) evolution. Using a realistic MJO simulation by incorporating the role of mesoscale stratiform heating in the Zhang-McFarlane deep convection scheme in the National Center for Atmospheric Research Community Atmosphere Model version 5.3 (NCAR CAM5.3), this study investigates factors responsible for the improved MJO simulation by examining moisture variations during different MJO phases. Results of column moist static energy (MSE) and moisture budgets show that during suppressed phases of MJO vertical advection acts to increase MSE anomalies for the development of deep convection while radiative heating and surface heat flux decrease MSE. The opposite holds true at MJO mature phase. However, their roles largely cancel each other, leaving horizontal advection to play a major role in low-level MSE increase during the suppressed phase of MJO and MSE decrease after the MJO mature phase. A further analysis combining moisture and temperature budget equations is performed to demonstrate the effects of vertical advection and cloud processes within the column at each level. The vertical profiles of column confined moisture tendency show that large-scale vertical advection induced by latent heat release and evaporation within shallow convective clouds is also important to the lower tropospheric moistening during suppressed phases. This confirms the role of shallow convection in low level moistening ahead of MJO deep convection. Radiative heating is vital across all MJO phases and its warming effects keep the column humidity anomaly maintained in mature phases. None of these features are reproduced by the standard CAM5.3.

1. Introduction

The Madden-Julian Oscillation (MJO) has been studied extensively since it was first discovered by Madden and Julian (1971, 1972) because of its important impacts on tropical and global climate. The MJO is characterized by an envelope of enhanced, highly organized deep convection and precipitation propagating eastward from the Indian Ocean to the Western Pacific at about 5 m/s (Zhang, 2005, 2013). Although significant progress has been achieved in many aspects (e.g. the multiscale structure and geographical preference of MJO) and several theories (e.g. considering MJO as an atmospheric response to independent forcing or atmospheric instability) have been developed to understand the MJO dynamics (Zhang, 2005, 2013; Li, 2014; Li et al., 2020; C. Zhang et al., 2020), MJO simulation remains poor in most of the global climate models (GCMs) (e.g. Hung et al., 2013; Wang et al., 2017, 2018; Le et al., 2021). Many observational (e.g. Sherwood, 1999; Wang and Li, 2020) and modeling (e.g. Grabowski, 2003; Derbyshire et al., 2004) studies have shown that moisture variation plays a critical role in controlling convection. Thus, a thorough understanding of moisture variation in MJO evolution is useful for improving the simulation of convection associated with MJO in numerical models.

Two main theories have been proposed to explain moisture variation during MJO evolution. One treats MJO as a moisture mode, in which the associated growth of convection is characterized by changes of anomalous moisture (e.g. Maloney, 2009; Hannah and Maloney, 2011; Sobel and Maloney, 2013; Adames and Maloney, 2021) under weak temperature gradient (WTG) approximation (Sobel et al., 2001). It can be quantified with gross moist stability (GMS, Neelin and Held, 1987) defined originally as the export of vertically integrated moist static energy (MSE). A normalized GMS was later proposed by Raymond et al. (2009). The enhanced MJO with negative GMS would suggest the instability of moisture mode. In other words, the variation of moisture could diagnose the development and distribution of convection. The other is based on a recharge-discharge mechanism (Benedict and Randall, 2007), in which the column integrated MSE builds up, leading to the generation of deep convection, and gradually decreases once precipitation forms (e.g. Maloney, 2009). In this view, the region to the east of existing MJO is favored by the recharging processes to moisten the low-level troposphere during suppressed convective period. When convection deepens, the free tropospheric moisture is discharged through precipitation. Although the fundamental mechanism to both the moisture mode framework and the recharge-discharge framework is the interaction between convection and free-tropospheric moisture, these two theories have clear differences in their interpretation on the control mechanism of free-tropospheric humidity variations and the way anomalous moisture and convection interact. In nature, the enhancement of column integrated MSE is initiated from the generation of shallow convection and horizontal advection, which increases the low-level positive moisture anomalies, enhancing the development of deep convection. As argued by Chikira (2014) and Wolding and Maloney (2015), moisture mode theory emphasize the important role of shallow convection on maintaining the existing instability through the amplification of moisture by column processes. On the other hand, the recharge-discharge theory treats the role of shallow convection as gradual moistening.

The MSE has been widely used to understand how moisture varies in intraseasonal oscillations and other tropical perturbations in GCMs and observations (e.g. Back and Bretherton, 2006; Maloney, 2009; Maloney et al., 2010; Kiranmayi and Maloney, 2011; Hannah and Maloney, 2011; Andersen and Kuang, 2012; Cai et al., 2013). Different terms in the column MSE budget equation have distinct contributions to MJO propagation. For instance, horizontal and vertical advection works to increase the instability while surface turbulent fluxes and radiative heating stabilize the MJO at suppressed phases (e.g. Kiranmayi and Maloney, 2011). The ultimate goal of MSE budget analysis is to understand how the net moisture tendency varies in a column because under the WTG approximation the MSE budget becomes the moisture budget. In this regard, an analysis approach proposed by Chikira (2014) on the vertical profile of moisture change within the column is useful for understanding the moisture variation. His results confirm the importance of horizontal advection in MJO eastward propagation and point out the crucial role of external heating (cooling) such as radiative heating (cooling) in moistening (drying) through large-scale vertical motion. Later work along this line of research using reanalysis and superparameterization provides new perspectives on why a small source of moisture anomaly might be critical to MJO amplitude by diagnosing vertical motion from diabatic heating (Wolding and Maloney, 2015; Wolding et al., 2016). Adames (2017) also expanded on the work of Chikira (2014), showing that the moisture tendencies accurately describe the observed distribution of MJO-related rainfall. Using a cloud-resolving model (CRM) simulation during the Dynamics of the Madden-Julian Oscillation (DYNAMO) project, Janiga and Zhang (2016) noted that low-level moistening ahead of MJO passage results from shallow convection. By modifying the cumulus parameterization in Weather Research Forecasting (WRF), Liu et al. (2022) found improved simulation of MJO propagation. This was attributed to the enhanced feedback between shallow convection and low-level moisture convergence, which result in amplified shallow convective heating.

Although the role of shallow convection in moistening the environment for the development of MJO-associated deep convection has been demonstrated in many studies (e.g. Mapes, 2000; Slingo et al., 2003; Zhang and Mu, 2005; Mu and Zhang, 2008; Zhang and Song, 2009; Hsu and Li, 2012; Hsu et al., 2014; Cao and Zhang, 2017; Shin and Baik, 2023), there are still many unanswered questions. For example, how does enhanced shallow convection in the suppressed phases of MJO serve to moisten the lower atmosphere exactly? How does vertical advection interact with convective cloud processes during MJO lifecycle? This study investigates the moisture variation during the MJO evolution using simulations from Cao and Zhang (2017) (hereafter CZ17). By incorporating mesoscale stratiform heating structure in the Zhang-McFarlane deep convection scheme in an NCAR CAM5 simulation (referred to as BOTC hereafter, as in CZ17), CZ17 found that the characteristics of the simulated MJOs compare well with those in observations. The substantial improvements in the BOTC run compared to the standard CAM5 run (referred to as the CTRL run) were evaluated thoroughly in CZ17. It was mainly attributed to increased shallow convection ahead of deep convection during suppressed phases, which moistens the lower troposphere by vertical advection. However, how the shallow convection facilitates the MJO development during suppressed phases and the exact physical mechanism of moisture variation during the MJO lifecycle are still unclear. Given the importance of moisture variations in the MJO life cycle, in this study, we will use the framework from Chikira (2014) based on WTG approximation to diagnose the impact of mesoscale heating profile on the formation of the MJO-scale moisture anomalies in the MJO simulations in CAM5.3. Under this framework, how modified convective parameterization improves the MJO simulation can be revealed through column processes analysis. Recently, Chen et al. (2021) also implemented a mesoscale convective heating parameterization similar to that in CZ17 into the DOE E3SM v1 and found similar improvement in MJO simulation. Thus, the results from this study may be applicable to other GCMs as well.

The remainder of the paper is organized as follows. The model, analysis method and data used in this study are described in section 2. Section 3 provides the results of moisture variation and gives insights on how moisture varies during MJO by using column MSE budget and the vertical profile of column confined moisture budget. Discussion and conclusions are presented in section 4.

2. Model, method, and data

The standard version of the National Center for Atmospheric Research Community Atmosphere Model version 5.3 (NCAR CAM5.3) is used in this study. It has a vertical resolution of 30 levels and a horizontal resolution of 1.9°× 2.5° (Neale et al., 2010). The planetary boundary layer parameterization uses a diagnostic turbulent kinetic energy based scheme (Bretherton and Park, 2009). Shallow convection is represented by Park and Bretherton (2009), and deep convection is parameterized by the Zhang-McFarlane scheme (Zhang and McFarlane, 1995, hereafter ZM).

This study examines the moisture variation at MJO-scale by analyzing the heat and moisture budgets, which in pressure coordinates are given by

$$\frac{\partial \bar{s}}{\partial t} + \bar{\boldsymbol{V}}_h \cdot \nabla \bar{s} + \bar{\omega}\frac{\partial \bar{s}}{\partial \mathrm{p}} = L(c-e) + \bar{Q}_R - \frac{\partial \overline{\omega' s'}}{\partial \mathrm{p}} \quad (1)$$

$$\frac{\partial \bar{q}}{\partial t} + \bar{\boldsymbol{V}}_h \cdot \nabla \bar{q} + \bar{\omega}\frac{\partial \bar{q}}{\partial \mathrm{p}} = -(c-e) - \frac{\partial \overline{\omega' q'}}{\partial \mathrm{p}} \quad (2)$$

where $\bar{s} = C_p\bar{T} + g\bar{z}$ is dry static energy, $\bar{q}$ is specific humidity, C_p and L denote specific heat at constant pressure and latent heat of vaporization, respectively. c is condensation rate, e is evaporation rate, $\bar{\boldsymbol{V}}_h$ represents horizontal velocity vector, $\bar{\omega}$ is vertical velocity, $\bar{Q}_R$ represents radiative heating, and $-\frac{\partial \overline{\omega' s'}}{\partial \mathrm{p}}$ and $-\frac{\partial \overline{\omega' q'}}{\partial \mathrm{p}}$ are the eddy transport of DSE and moisture, respectively. Overbar denotes average over the GCM grid box. $\bar{Q}_R$ can be written in flux form as $\mathrm{g}\frac{\partial F_R}{\partial \mathrm{p}}$, where F_R is radiative flux. $-\frac{\partial \overline{\omega' s'}}{\partial \mathrm{p}}$ and $-L\frac{\partial \overline{\omega' q'}}{\partial \mathrm{p}}$ can be written as $\mathrm{g}\frac{\partial F_s}{\partial \mathrm{p}}$ and $\mathrm{g}\frac{\partial F_L}{\partial \mathrm{p}}$, where F_s and F_L are the sensible and latent heat fluxes due to subgrid scale eddies, presumably by convection in the free troposphere and turbulence in the boundary layer. Combining Eqs. (1) and (2) gives the MSE budget equation,

$$\frac{\partial \bar{h}}{\partial t} = -\bar{\boldsymbol{V}}_h \cdot \nabla \bar{h} - \bar{\omega}\frac{\partial \bar{h}}{\partial p} + \mathrm{g}\frac{\partial F_L}{\partial \mathrm{p}} + \mathrm{g}\frac{\partial F_s}{\partial \mathrm{p}} + \mathrm{g}\frac{\partial F_R}{\partial \mathrm{p}} \quad (3)$$

where $\bar{h} = \bar{s} + L\bar{q}$ is MSE.

One way to understand how tropospheric specific humidity is affected by various processes during MJO is to use column integrated MSE. The vertically integrated $\bar{h}$ budget can be formally written from Eq. (3) as (Neelin and Held, 1987; Maloney, 2009; Kiranmayi and Maloney, 2011),

$$< \frac{\partial \bar{h}}{\partial t} >= -< \bar{\boldsymbol{V}}_h \cdot \boldsymbol{\nabla} \bar{h} > -< \bar{\omega} \frac{\partial \bar{h}}{\partial p} > + LH + SH + < LW > + < SW > \quad (4)$$

where the angle brackets denote mass-weighted column integral from the surface to the top of the atmosphere, $< x >= \frac{1}{g}\int_{P_T}^{P_B} x dp$. $< \frac{\partial \bar{h}}{\partial t} >$ represents the vertically integrated $\bar{h}$ tendency, the first and second terms on the right-hand side (rhs) represent the column integrated export of $\bar{h}$ due to horizontal and vertical advections, $< LW >$ and $< SW >$ are the net longwave and shortwave fluxes into the atmosphere, LH and SH are the surface latent and sensible heat fluxes.

Eqs. (1) and (2) can also be combined to examine the moisture field under the weak temperature gradient (WTG) approximation (Sobel et al., 2001) following Chikira (2014). When the eddy transport terms due to convection are expressed explicitly in terms of convective mass flux and detrainment, Eqs. (1) and (2) can be rewritten as (Yanai et al., 1973; Chikira, 2014; Janiga and Zhang, 2016),

$$\frac{\partial \bar{s}}{\partial t} + \bar{\boldsymbol{V}}_h \cdot \boldsymbol{\nabla} \bar{s} + \bar{\omega} \frac{\partial \bar{s}}{\partial \mathrm{p}} = \bar{D}_s - M_c g \frac{\partial \bar{s}}{\partial \mathrm{p}} + \tilde{Q}_i + L(\tilde{c} - \tilde{e}) + \bar{Q}_R + \bar{S}_{df} \quad (5)$$

$$\frac{\partial \bar{q}}{\partial t} + \bar{\boldsymbol{V}}_h \cdot \boldsymbol{\nabla} \bar{q} + \bar{\omega} \frac{\partial \bar{q}}{\partial \mathrm{p}} = \bar{D}_q - M_c g \frac{\partial \bar{q}}{\partial \mathrm{p}} - (\tilde{c} - \tilde{e}) + \bar{Q}_{df} \quad (6)$$

where $\tilde{c}$ is large-scale condensation rate, $\tilde{e}$ is evaporation of large-scale precipitation in the environment, $\bar{D}_q$ and $\bar{D}_s$ are tendencies due to detrainment from convection, $M_c = \rho\sigma w_c$ is the net convective mass flux, $\tilde{Q}_i$ is latent heating from liquid-ice phase transition, $\bar{S}_{df}$ and $\bar{Q}_{df}$ are heating and moistening from vertical diffusion. Tildes denote the mean value outside of convection in a grid box (environment). By definition, the grid-mean vertical velocity is the sum of mass flux inside convection and vertical velocity in the convection environment:

$$\bar{\omega} = -M_c g + \tilde{\omega} \quad (7)$$

where $\tilde{\omega}$ is environmental vertical velocity. Substituting $\bar{\omega}$ in Eq. (7) into Eqs. (5) and (6) gives,

$$\frac{\partial \bar{s}}{\partial t} + \bar{\boldsymbol{V}}_h \cdot \boldsymbol{\nabla} \bar{s} + \tilde{\omega} \frac{\partial \bar{s}}{\partial \mathrm{p}} = \bar{D}_s + \tilde{Q}_i + L(\tilde{c} - \tilde{e}) + \bar{Q}_R + \bar{S}_{df} \quad (8)$$

$$\frac{\partial \bar{q}}{\partial t} + \bar{\boldsymbol{V}}_h \cdot \boldsymbol{\nabla} \bar{q} + \tilde{\omega} \frac{\partial \bar{q}}{\partial \mathrm{p}} = \bar{D}_q - (\tilde{c} - \tilde{e}) + \bar{Q}_{df} \quad (9)$$

By applying the WTG approximation, Eq. (8) takes the following form,

$$\tilde{\omega} \frac{\partial \bar{s}}{\partial \mathrm{p}} = \bar{D}_s + \tilde{Q}_i + L(\tilde{c} - \tilde{e}) + \bar{Q}_R + \bar{S}_{df}$$

or

$$\tilde{\omega} = \left(\frac{\partial \bar{s}}{\partial \mathrm{p}}\right)^{-1} [\bar{D}_s + \tilde{Q}_i + L(\tilde{c} - \tilde{e}) + \bar{Q}_R + \bar{S}_{df}] \quad (10)$$

With this, Eq. (9) can be rewritten as,

$$\frac{\partial \bar{q}}{\partial t} = -\bar{\boldsymbol{V}}_h \cdot \boldsymbol{\nabla}\bar{q} - \tilde{\omega}\frac{\partial \bar{q}}{\partial \mathrm{p}} + \bar{D}_q - (\tilde{c} - \tilde{e}) + \bar{Q}_{df} = -\bar{\boldsymbol{V}}_h \cdot \boldsymbol{\nabla}\bar{q} + \left(\frac{\partial \bar{q}}{\partial t}\right)_{column} \quad (11)$$

where

$$\left(\frac{\partial \bar{q}}{\partial t}\right)_{column} = -\tilde{\omega}\frac{\partial \bar{q}}{\partial p} + \bar{D}_q - (\tilde{c} - \tilde{e}) + \bar{Q}_{df}$$

$$= \left(\frac{\partial \bar{q}}{\partial p}\right)\left(\frac{\partial \bar{s}}{\partial \mathrm{p}}\right)^{-1}\left[\bar{D}_s + \tilde{Q}_i + L(\tilde{c} - \tilde{e}) + \bar{Q}_R + \bar{S}_{df}\right] + \bar{D}_q - (\tilde{c} - \tilde{e}) + \bar{Q}_{df}$$

$$= (\alpha - 1)(\tilde{c} - \tilde{e}) + \frac{\alpha}{L}(\bar{Q}_R + \tilde{Q}_i) + (\bar{D}_q + \frac{\alpha}{L}\bar{D}_s) + (\bar{Q}_{df} + \frac{\alpha}{L}\bar{S}_{df}) \quad (12)$$

where

$$\alpha = -L\left(\frac{\partial \bar{q}}{\partial p}\right)\left(\frac{\partial \bar{s}}{\partial \mathrm{p}}\right)^{-1}$$

and

$$\alpha - 1 = -\left(\frac{\partial \bar{s}}{\partial \mathrm{p}}\right)^{-1}\left[\mathrm{L}\left(\frac{\partial \bar{q}}{\partial \mathrm{p}}\right) + \left(\frac{\partial \bar{s}}{\partial \mathrm{p}}\right)\right] = -\left(\frac{\partial \bar{h}}{\partial \mathrm{p}}\right)\left(\frac{\partial \bar{s}}{\partial \mathrm{p}}\right)^{-1} \quad (13)$$

measures the ratio of the lapse rate of moist static energy to that of dry static energy. In the lower troposphere $\partial\bar{h}/\partial p > 0$, thus $\alpha - 1 > 0$; in the upper troposphere $\partial\bar{h}/\partial p < 0$, thus $\alpha - 1 < 0$ since $\left(\frac{\partial \bar{s}}{\partial \mathrm{p}}\right)^{-1}$ is negative for stable atmosphere. $\alpha - 1$ characterizes the efficiency of moistening (drying) at a given level by vertical advection through vertical motion induced by the external heating (cooling). It is related to the original definition of the GMS by Neelin and Held (1987) and the shallow water GMS described by Sobel and Maloney (2013) and Adames and Kim (2016).

The net effect of vertical advection, cloud processes and vertical diffusion within a column is referred to as "column process" by Chikira (2014) since these processes are confined to a single atmospheric column. The first term on the rhs of Eq. (12) represents the net effect of condensation minus evaporation in the convection environment (e.g. stratiform). When there is net condensation in the lower troposphere, it moistens the atmosphere. While this goes counterintuitive, it can be understood if the atmospheric motion is considered together with the WTG approximation. In the lower troposphere when there is condensation, the condensational heating generates an upward motion such that the heating is balanced by the adiabatic cooling. The upward motion leads to moistening from vertical advection that overpowers the condensation due to strong vertical gradient in moisture, thereby leading to net moistening. In the upper troposphere, due to weak vertical moisture gradient, condensation leads to net drying, as expected from conventional thinking. The second, third and last terms on the rhs of Eq. (12) are moistening due to the sum of radiative heating and freezing heat, detrainment of moisture and DSE, and moisture and heat diffusion, respectively. All the diabatic heating terms (e.g. radiative heating) affect moisture through the implied vertical advection by the heating-induced vertical motion. Thus, analyzing the moisture budget in terms of the column process is not only consistent with the column MSE budget, but also provides extra benefits by quantifying the effects of individual processes at specific levels on moisture variation, especially in the lower troposphere, which are important for MJO convection. Processes quantified under this framework include radiation, detrainment of heat and moisture and microphysical process in the convection environment.

The composite anomalous terms of Eqs. (4), (11) and (12) as a function of MJO phases are shown in the following section. The anomalies of all fields are obtained by subtracting the annual means from their absolute values and applying a 20-100-day Lanczos bandpass filter. The composite phases are determined from Real-time Multivariate MJO series (RMM) method (Wheeler and Hendon, 2004). The analysis focuses on boreal winter (November to April) over the tropics. From the spectral and multivariate EOF analyses in CZ17, it was found that MJOs in observations reach the mature phase in the Indian Ocean whereas MJOs in the CAM5.3 simulations reach the mature phase near the Maritime Continent (cf. Fig.4 in CZ17). In order to compare them properly in both simulations and observations and analyze the associated characteristics, we take a phase-centric view rather than a location-centric view. In other words, we compare the observed MJO at its mature phase in the Indian Ocean with simulated MJO at its mature phase near the Maritime Continent. If we were to compare observed and simulated MJOs at the same location, say, the Indian Ocean, we would end up comparing the mature phase of the observed MJO with the developing phase of the simulated MJO, which would not be an apple-to-apple comparison. As such, the model results are longitudinally averaged over Maritime Continent (115-125°E,10°S-10°N) while observations are over Indian Ocean (85-95°E, 10°S-10°N) where MJO peaks. Note that the selection of different location between observations and model simulations may lead to some discrepancies in the role of horizontal advection due to differences in basic states at different locations. Recently, Mayta and Adames Corraliza (2023) found that the moisture mode is more applicable over Indian ocean and less so over western Pacific and Maritime Continent. Nonetheless, the comparison between the two model simulations is at the same location, and thus is not affected by any geographical shift in the simulated mean state between CTRL and

BOTC. Taking a phase-centric view is consistent with the composite analysis of MJO results in different phases.

The datasets used to evaluate the model performance include daily European Centre for Medium range Weather Forecasts (ECMWF) interim reanalysis data (ERA-interim, hereafter refer to as ERA-I, Simmons et al., 2007), daily TRMM precipitation product (Huffman et al., 2007) and daily GPCP product (Huffman et al., 2001). As in CZ17, there are two AMIP model simulations: the standard NCAR CAM5 run (CTRL) and the experiment with stratiform heating which includes an upper-level heating and a lower-level cooling to mimic the heating profile from the stratiform part of mesoscale convective systems (BOTC). Specifically, in BOTC we artificially modified the vertical structure of heating profile in convective parameterization scheme in CAM5.3. A stratiform heating from condensation in the upper level and cooling from rain evaporation in the lower levels are incorporated into the original convective heating profile, with the column integrated total heating conserved. The inclusion of stratiform heating enhanced the shallow convection in the simulation, which leads to a better simulation of MJO in both magnitude and eastward propagation. More details about the difference between CTRL and BOTC can be found in CZ17. Both reanalysis data and model simulations are from years 1992 to 2001.

3. Results

3.1 Characteristics of moisture variation during MJO evolution

The vertical profiles of specific humidity anomalies at each phase on MJO-scales are shown in Fig. 1. In both observations and simulations, the gradual evolution of moisture is consistent with previous studies (e.g. Cai et al., 2013; Hsu et al., 2014) in which negative moisture anomalies occur at suppressed and dissipating phases while positive moisture anomalies increasingly appear from developing to mature phases. The positive moisture anomaly peaks near 500hPa in the mature stage (around Phase 5) while the negative one peaks near the same height at Phase 8 in ERA-I and both simulations. Both ERA-I and BOTC have much larger amplitudes of moisture anomalies in almost the entire column, especially from 700hPa to 400hPa, compared with CTRL. Especially, the transition phases are shown in both ERA-I and BOTC where Phase 2 (6) has low-level positive (negative) and upper-level negative (positive) anomalies. The lack of such shallow moistening ahead of the main MJO development phase in CTRL may directly lead to the poor MJO simulation. In addition, we note that compared with ERA-I, both simulations show much smaller magnitudes of moisture anomalies below 850hPa. Previous studies (e.g. Benedict and Randall, 2011; Cai et al., 2013; DeMott et al., 2015) have suggested that the positive feedback between the atmosphere and the ocean is important to intraseasonal variability. Thus, one possible cause may be the prescribed SST in the AMIP simulations. Another possibility is that the planetary boundary layer (PBL) parameterization used in CAM5 cannot generate enough vertical transport in PBL or lack of moisture convergence from surface friction.

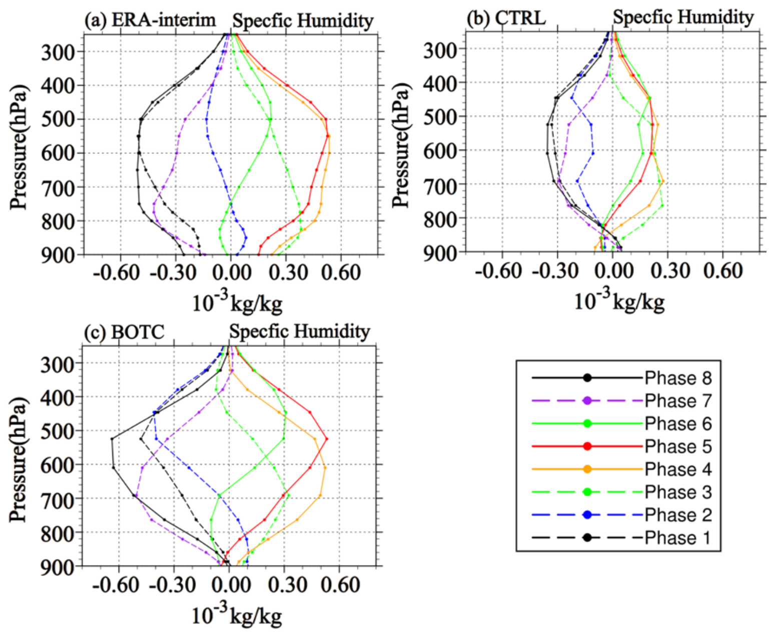

Fig. 1. Composite of vertical profiles of specific humidity anomalies on the MJO scale at each phase averaged over eastern Indian Ocean (85-95°E, 10°S-10°N) for (a) ERA-interim; and Maritime Continent (115-125°E, 10°S-10°N) for (b) CTRL and (c) BOTC. Lines in different colors represent different phases.

The column-integrated MSE is critical to MJO evolution (e.g. Maloney, 2009; Kiranmayi and Maloney, 2011). Fig. 2 shows the variation of column-integrated MSE vs. that of specific humidity and dry static energy (DSE) during the 8 phases of MJO development for ERA-I reanalysis data and the two simulations. The symbols connected with arrows indicate the MJO evolution from phase 1 to phase 8. The MSE variations in different phases of the MJO mostly come from moisture anomalies. However, DSE anomalies, although relatively small, are significant, nonetheless. The moisture mode theory posits that MSE anomalies are approximately governed by moisture anomalies (Mayta and Adames Corraliza, 2023). Thus, significant DSE variations from one phase to another suggest that the moisture mode theory only holds approximately. The moisture variation is compensated by DSE variation, such that the MSE anomalies are positively correlated with moisture anomalies but negatively correlated with DSE anomalies as the MJO evolves. During the inactive or suppressed phases (phases 1, 2, 7 and 8) of the MJO over the Maritime Continent, MSE and moisture anomalies are negative while during the active phases (phases 3, 4, 5 and 6) the anomalies are positive. Strong similarities in distribution and magnitude are also found in the phase-longitude distribution of vertically integrated MSE and that of specific humidity (not shown), suggesting that the variations in MSE on MJO-scale are mostly governed by moisture variation. These are consistent with several previous studies (e.g. Maloney, 2009; Kiranmayi and Maloney, 2011; Andersen and Kuang, 2012). In both ERA-I and BOTC simulation, at the MJO initial phase (phases 1&2) the moisture anomaly is negative and the DSE anomaly is positive, but to a lesser extent, resulting in a positive MSE anomaly. Afterwards, the column integrated MSE increases (as a result of increased moisture overwhelming decreased DSE) until phase 4. After the MJO reaches its mature phase, MSE and moisture anomalies start to decrease. It indicates an energy build-up and consumption process during the MJO lifecycle. There is an asymmetry between developing and decaying phases of MJO in moisture and DSE anomalies. The atmosphere is drier and warmer in the developing phase, but moister and cooler in the decaying phase. Therefore, the progression around the origin follows a counterclockwise trajectory for moisture anomalies and a clockwise trajectory for DSE anomalies. However, the CTRL run shows an opposite behavior.

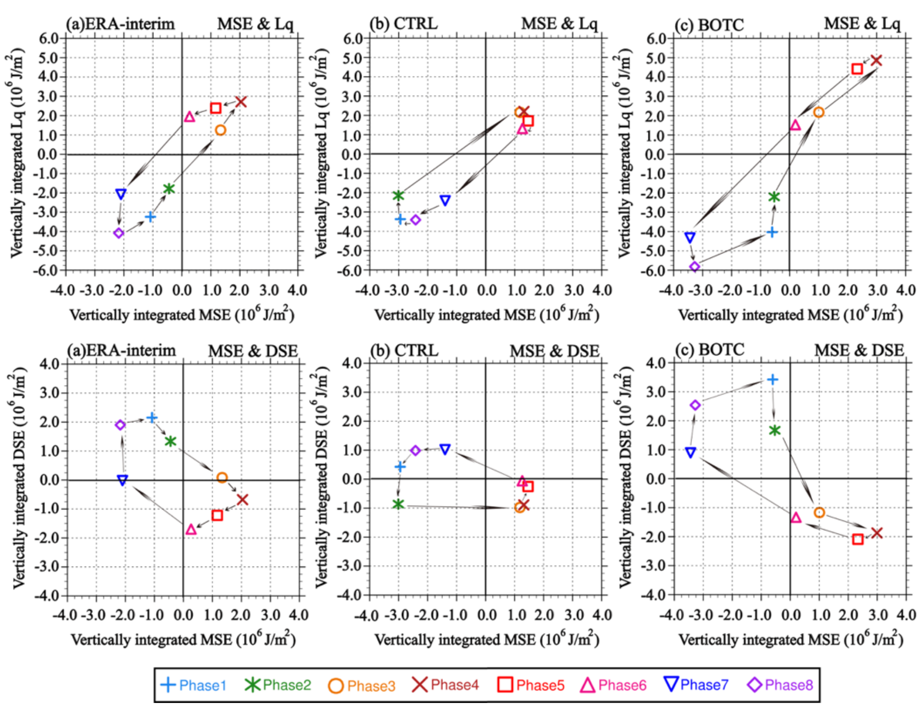

Fig. 2. Phase space diagram of vertically integrated MSE, Lq (first row), and DSE (second row) anomalies as a function of MJO phases averaged over eastern Indian Ocean (85-95°E, 10°S-

10°N) for (a) ERA-interim; and Maritime Continent (115-125°E, 10°S-10°N) for (b) CTRL and (c) BOTC. Different symbols represent different phases.

3.2 MSE budget analysis

The moisture and MSE budget analysis as a tool is used to understand individual processes in the MJO evolution. The budget terms for the vertically integrated anomalous MSE in Eq. (4) during the MJO lifecycle are shown in Fig. 3. The vertically integrated MSE and precipitation anomalies are also shown. Note that MSE anomalies slightly lead precipitation anomalies (by one phase) in ERA-I and BOTC and are in phase with precipitation anomalies in CTRL. Overall, precipitation is tightly related to column water vapor, another assumption in moisture mode theory (Zhang et al., 2020), in both the reanalysis data and model simulations. In BOTC, positive precipitation anomalies appear at Phase 3 and peak at Phase 5, showing very close agreement with those in ERA-I. In the CTRL run, there are two peaks of anomalous precipitation with smaller amplitudes at Phases 3 and 6, implying deep convection develops too early. The dominant terms in the MSE budget are vertical advection and energy fluxes going into the atmosphere from the top and bottom, and they are largely opposite in signs. The effect of vertical motion on MSE is important for the maintenance of MSE anomalies in MJO lifecycle. In both ERA-I and BOTC vertical advection acts to maintain the MSE anomalies during the initial and early developing phases of MJO and stabilize the column during the mature phases. This reflects the fact that upward motion in the initial and developing phases can only reach a lower altitude. As a result, the associated mass convergence in the lower levels brings more energy into the column than the energy taken out by the mass divergence in the upper part of the upward motion layer. In the mature phase, upward motion reaches the upper troposphere. Consequently, the mass divergence in the upper troposphere exports more energy out of the column than the energy brought in by mass convergence in the lower troposphere. The variation of energy fluxes into the atmospheric column from the top and bottom decreases the column MSE in the early phases and increases the column MSE in mature phase.

Because of the large cancelation between vertical advection and energy fluxes into the atmospheric column from the top and bottom, MSE tendency largely follows MSE changes due to horizontal advection. This applies to both ERA-I and the CAM5 simulations although the magnitude of variation is smaller in CTRL. It should be noted that there is a residual after adding up all the budget terms, which has been addressed in previous research and attributed to misrepresentation of moistening process ahead of MJO in reanalysis model or inevitably errors between exact outputs of advection terms and vertical interpolation of standard variables (Neelin and Held, 1987; Maloney, 2009; Kiranmayi and Maloney, 2011).

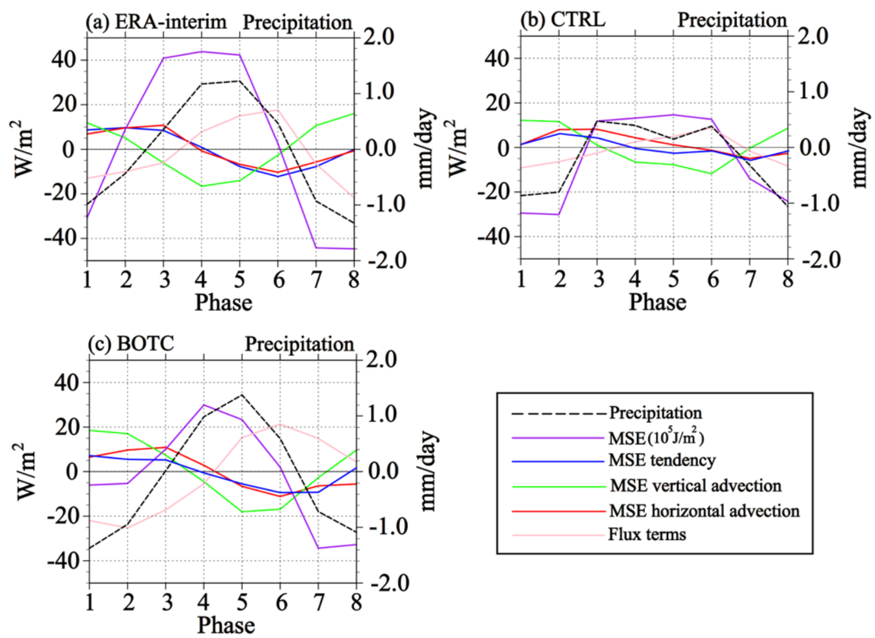

Fig. 3. Vertically integrated anomalous MSE budget terms (W/m^2) (solid lines in different colors) from the Eq. (1) averaged over eastern Indian Ocean (85-95°E, 10°S-10°N) for (a) ERA-interim; and Maritime Continent (115-125°E, 10°S-10°N) for (b) CTRL and (c) BOTC. Precipitation anomalies (mm/day, dash line and the right ordinate) and vertically integrated MSE (10^5J/m^2, purple line with the left ordinate) are also shown.

As the net energy flux into the atmospheric column is the dominant term that counteracts the vertical advection, Fig.4 further examines the contributions from its components, that is, shortwave, longwave, surface sensible and latent heat fluxes. The variation of the net flux is dominated by that of longwave flux, with secondary contribution from surface latent heat flux, while shortwave and sensible heat flux contributions are insignificant. The longwave flux is particularly large during initial and mature phases, more than twice as large as that of surface latent heat flux. In the early phases, cloud tops are low, and the cloud longwave effect is small. Thus, the atmospheric column loses more energy (relative to the climatological mean) by emitting longwave radiation at higher temperature. During and after the mature phase, cloud tops are high, and the longwave cloud radiative forcing is large. Thus, the atmosphere gains energy relative to the climatological mean. The surface latent heat flux anomalies in ERA-I are negative in the initial and developing phases of MJO and positive after phase 5, becoming negative near the end of the MJO lifecycle. In BOTC, the latent heat flux anomalies are negative before phase 5 and positive after phase 5, with a larger magnitude than that in ERA-I. In CTRL, latent heat flux anomalies are small in all phases of the MJO.

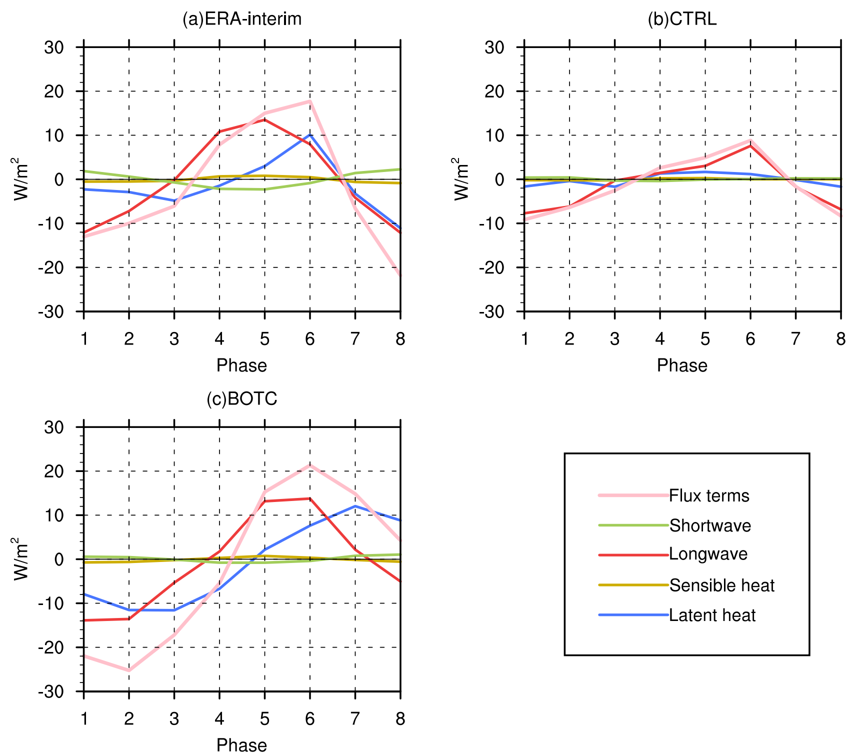

Fig. 4. Vertically integrated anomalous flux terms (pink solid lines) and its decomposition averaged over eastern Indian Ocean (85-95°E, 10°S-10°N) for (a) ERA-interim; and Maritime Continent (115-125°E, 10°S-10°N) for (b) CTRL and (c) BOTC.

In Fig. 5, both ERA-I and BOTC show that the net MSE tendency is located ahead of precipitation anomalies, leading by about 90° of MJO phases. Such quadrature distribution indicates that the maintenance and dissipation of column MSE anomalies before and after the MJO precipitation drive the eastward propagation of the MJO convective center. This result is consistent with previous reanalysis (e.g. Kiranmayi and Maloney, 2011). In CTRL, although there are also positive MSE anomalies ahead of precipitation anomalies, the precipitation anomalies do not coincide with the MJO propagation from the Indian Ocean to the Western Pacific. Horizontal advection (second row) helps to maintain column MSE anomalous ahead of MJO convection, but it only happens west of the Maritime Continent before Phase 4 and then the drying process takes over afterwards. In the view of moisture mode, MJO convection center is regarded as a moisture anomaly center. We found that the regions of negative vertical advection (third row) and positive flux terms (forth row) of MSE coincide with MJO convective center. It indicates that the moisture anomalies in MJO convection center is maintained in strength by the longwave radiation and surface latent heat flux but removed by vertical motions. The horizontal advection ahead of convective center act to propagate MJO eastward. As a result of the balance between surface fluxes and vertical advection, the net MSE tendency more resembling horizontal advection.

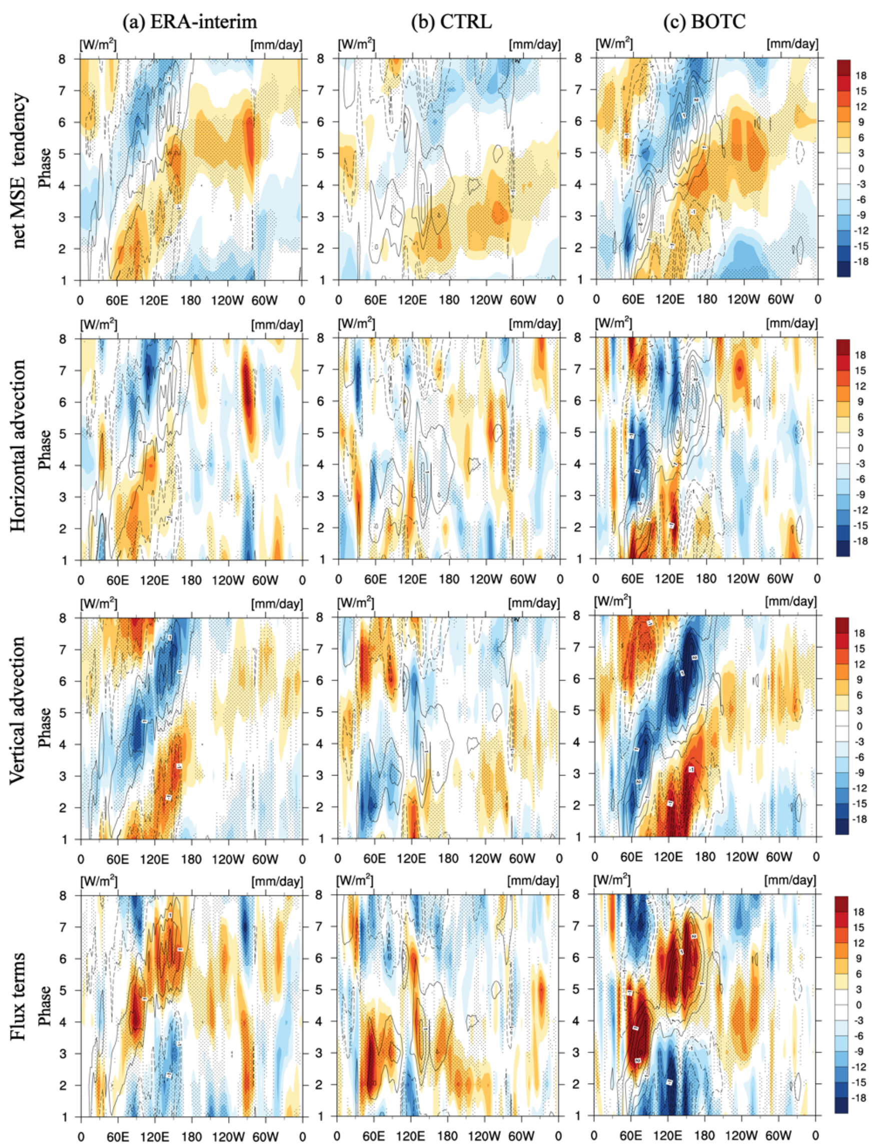

Fig. 5. Longitude-phase (averaged over 10°S-10°N) plots of vertically integrated anomalous MSE terms (W/m^2, color filled) for (a) ERA-interim; (b) CTRL; and (c) BOTC. Precipitation anomalies (mm/day, contours) are also drawn. Anomalies with a confidence level greater than 95% are stippled.

Fig. 6 shows the height-longitude cross section of anomalous MSE (color) and wind perturbations (vectors) in MJO active stage. An eastward extension of the MSE anomaly in the lower troposphere is seen in both ERA-I and BOTC, indicating that the lower tropospheric moistening occurs ahead of the MJO center. The 90°E longitude corresponds to the enhanced precipitation location in ERA-I at Phase 4. BOTC shows very similar features except located at 120°E where the peak precipitation occurs at Phase 5 in the model. Note that both ERA-I and BOTC show well-organized MSE anomalies, with a typical MJO easterly wind perturbation feeding into convection from ahead of the convection and westerly wind anomalies from the west. The positive specific humidity anomalies appear where there is a deep layer of positive MSE anomalies associated with strong upward motion. CTRL fails to capture such well-organized features. Wang et al. (2018) suggested that the horizontal structure of the lower tropospheric moistening and equatorial asymmetry of zonal wind favors eastward propagation.

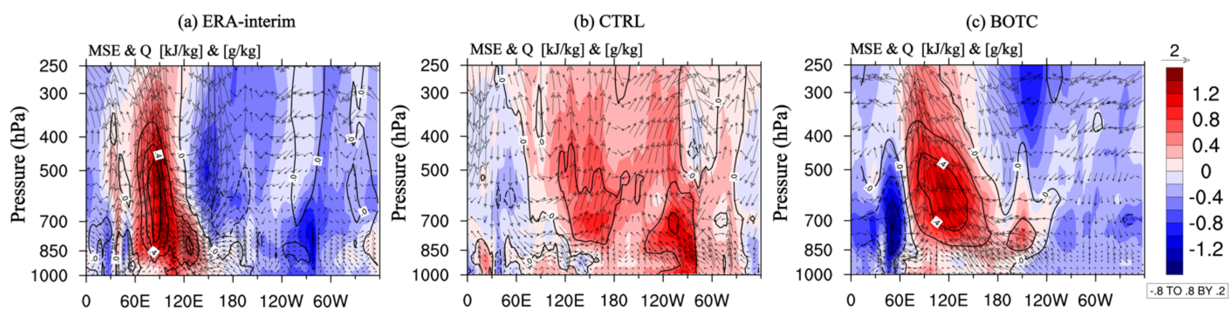

Fig. 6. Height-longitude cross sections of anomalous MSE (color filled, kJ/kg), specific humidity (contours, g/kg) and wind (u, w vectors, m/s) of composite MJO at Phase 4 for (a) ERA-interm and at Phase 5 for (b) CTRL and (c) BOTC.

3.3 Vertical structure of moisture budget

As shown in the last subsection, the horizontal advection contributes to the maintenance of MSE anomalies ahead of MJO convective center. A further breakdown of horizontal advection into zonal and meridional component (not shown) indicates that zonal advection dominates the MSE maintenance process and leads to the eastward propagation. Although some studies (e.g. Maloney, 2009; Kiranmayi and Maloney, 2011; Kim et al., 2014) pointed out that horizontal advection might be governed by meridional advection, our work indicates a larger influence from zonal advection, which is consistent with some other previous works (Hsu and Li, 2012; Liu and Wang, 2016; Kim et al., 2017). While vertical advection is large in the column integrated MSE budget, it is largely balanced by energy flux contributions from the top and bottom of the atmospheric column. Similarly, for moisture, although vertical advection from upward motion moistens the atmosphere, its accompanying condensation acts to dry the atmosphere (e.g. Benedict and Randall, 2007; Hsu and Li, 2012; Adames and Wallace, 2015). The net effect can be either moistening or drying depending on which process is more effective. From the WTG approximation Eq. (10), any diabatic process will affect vertical motion. To consider these processes explicitly in the framework of vertical advection, Chikira (2014) introduces the so-called "column process" or "column confined moisture tendency" as referred to by Janiga and Zhang (2016), which represents the net effect of vertical motion and all diabatic processes within a column that affect the moisture field. Wolding and Maloney (2015) and Wolding et al. (2016) used this method to estimate the vertical velocity resulting from each column process and investigate the moisture variation in the ERA-I reanalyses and the superparameterization version of CAM (SPCAM).

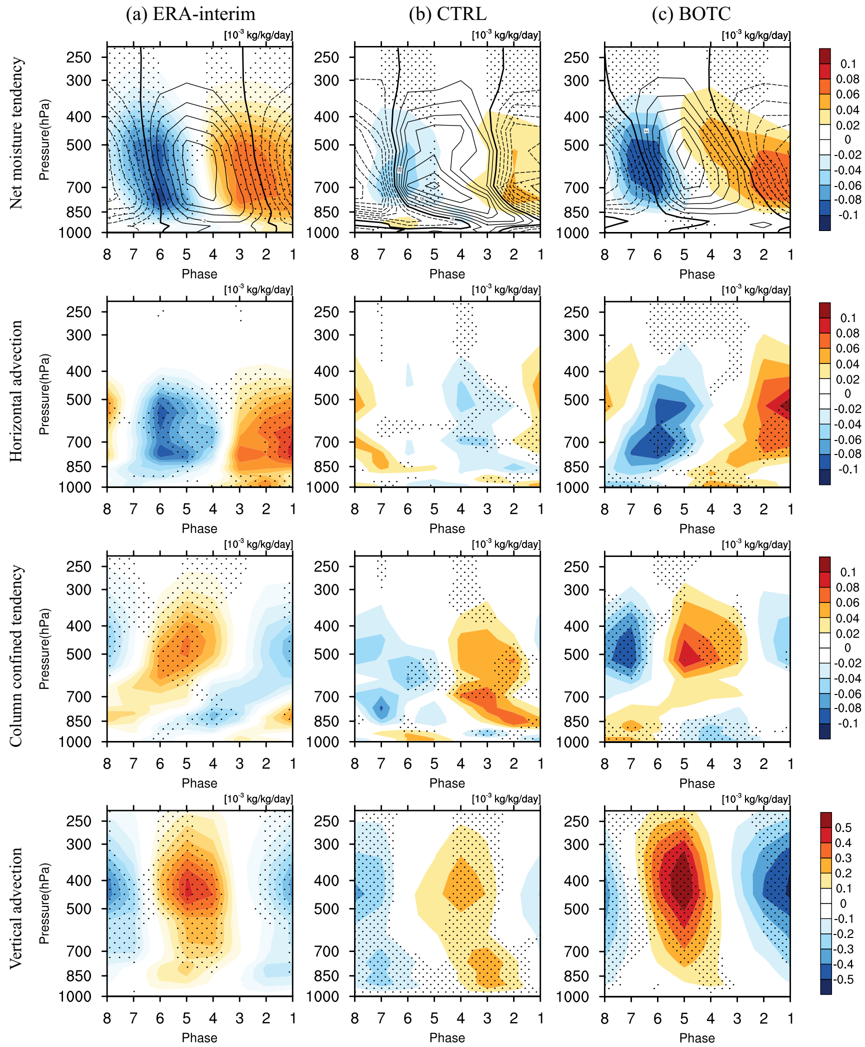

Fig. 7. Height-Phase plot of composites of anomaly net specific humidity tendency (first row, 10^{-3}kg/kg/day), horizontal advection (second row), column confined moisture tendency (third row) and vertical advection (fourth row) averaged over eastern Indian Ocean (85-95°E, 10°S-10°N) for (a) ERA-interim; and Maritime Continent (115-125°E, 10°S-10°N) for (b) CTRL; and (c) BOTC. Specific humidity anomalies (10^{-3}kg/kg, contours) are also drawn in the first row for reference. Note the color scale in the vertical advection plots differs from the rest. Anomalies with a confidence level greater than 95% are stippled.

Fig. 7 shows the height-phase cross section of net moisture tendency, horizontal advection, and column confined tendency. Also shown is the vertical advection of moisture for reference and comparison, which will be made clear shortly. Both ERA-I and model simulations show a tilted vertical structure of moisture as MJO develops. There is a positive net moisture tendency (first row) ahead of positive moisture anomalies, indicating an enhancement of moisture anomalies before MJO convection. Both ERA-I and BOTC moisture tendency peaks around 600 hPa. CTRL show much weaker signals. The horizontal advection (second row) in ERA-I and BOTC moistens the atmospheric column in initial stages from Phase 1 to 3 and dries it after the MJO mature phase (phase 5) as the MJO is gradually dissipating. The patterns of horizontal advection show high resemblance to those of the net moisture tendency, indicating that horizontal advection is the main contributor to the net moisture tendency, consistent with Figs. 3 and 5. Its moistening effect over lower troposphere is also confirmed by the shallow positive anomalies in the vertical structure of MSE horizontal advection ahead of the deep layer of MSE anomalies in Fig. 6. The magnitude of column confined moisture tendency (third row) is slightly smaller than the net moisture tendency and horizontal advection. It reaches the maximum during the mature phases of MJO in mid-troposphere in both ERA-I and BOTC. CTRL shows very different phase timing; the peak occurs at phase 3, ahead of the positive moisture anomalies in column confined moisture tendency around 700 hPa, implying that convection develops too early. For comparison, vertical advection (fourth row) shows significantly larger magnitude of drying and moistening than that of the column confined moisture tendency, by a factor of 5 or more. Comparing Eqs. (2) and (11), the column confined moisture tendency is the sum of vertical advection, total condensation minus evaporation and eddy transport due to subgrid-scale convection. This clearly indicates that although vertical advection and diabatic physical processes can have large contribution to moisture anomalies individually. They are largely in balance, leaving a comparatively small net effect on the moisture fields. Therefore, considering them in isolation can be misleading when attributing the source of moisture anomalies. They result in drying in the free troposphere in MJO suppressed phases and moistening in the MJO mature phase. The column confined moisture tendencies in the boundary layer will not be discussed here since the WTG approximation only applied to the free troposphere.

To demonstrate more clearly the roles of each budget term in Eq. (11) in moisture tendency, we use the initial suppressed and mature phases of MJO as examples below. Fig. 8 shows the vertical profiles of moisture budget averaged in suppressed (first row, phase 1&2) and mature phases (second row, phase 5), respectively. During suppressed phases, both ERA-I and BOTC show relatively small positive values of column confined moisture tendency in the lower troposphere and drying anomalies in the upper troposphere. The net moisture tendency is positive in the whole troposphere and dominated by contributions from horizontal advection. This is consistent with the above results that there is moistening ahead of active convection and horizontal advection contributes the most. CTRL shows different structures with smaller amplitude, especially in the lower troposphere. When the MJO develops into the mature phase, the moisture budget is largely opposite to the initial phases. In the upper troposphere, both ERA-I and BOTC have large moistening. Horizontal advection depletes moisture while column confined moisture tendency moistens the column as a source, except below the 800 hPa height. In CTRL, horizontal advection moistens the atmosphere while column confined tendency dries the atmosphere, leading to net drying throughout the troposphere with weaker magnitude.

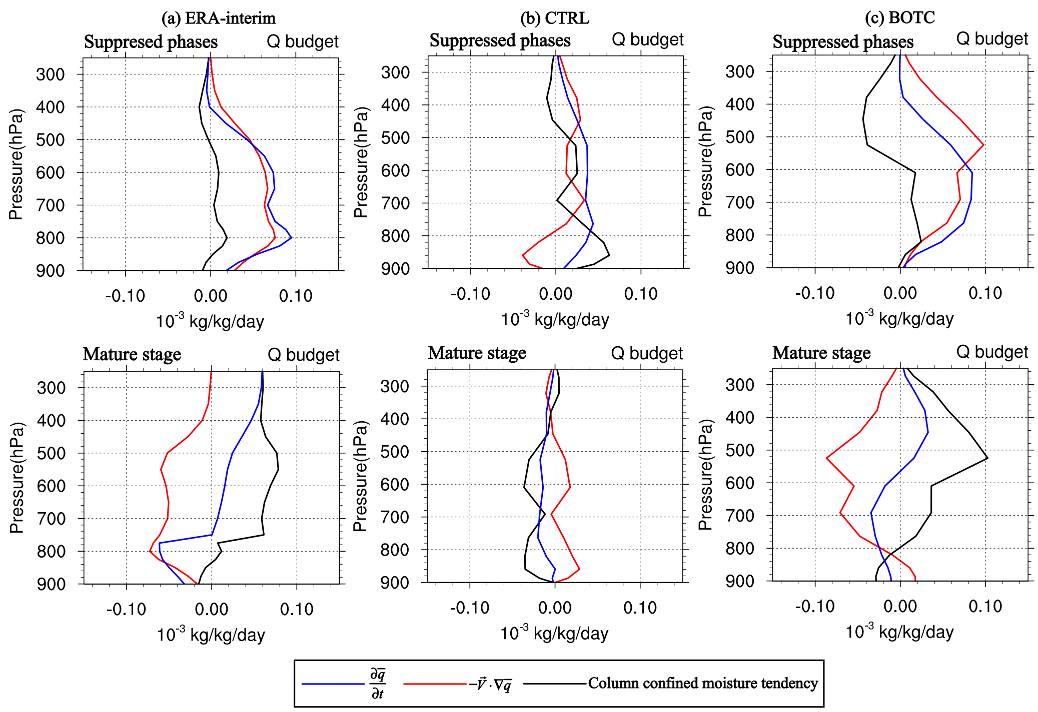

Fig. 8. Composite specific humidity budget terms in Eq. (11) (suppressed phases in first row, mature phase in second row), averaged over eastern Indian Ocean (85-95°E, 10°S-10°N) for (a) ERA-interim; and Maritime Continent (115-125°E,10°S-10°N) for (b) CTRL and (c) BOTC.

As horizontal advection is the dominant contributor to moistening in the lower and middle troposphere at the MJO initial phase and the main drying factor at the MJO mature phase, we further show horizontal maps of wind anomalies and mean specific humidity distributions at 700 hPa in Fig. 9 for MJO initial and mature phases. We found that the advection of mean specific humidity by anomalous wind plays a dominant role in the distribution and variation of horizontal advection, especially in the averaging area (not shown). The advection of anomalous specific humidity by mean wind contributes less except for areas north to 10°N. This is consistent with previous works (Cai et al., 2013; Kiranmayi and Maloney, 2011; Maloney, 2009). In ERA-I, the moisture maximum is centered east of 100°E. At the initial phase (Fig. 9a), the easterly winds bring moisture to the averaging domain (85-95°E, 10°S-10°N), leading to moistening. Conversely at phase 5, the westerly winds bring in dry air and cause drying in the region. In CTRL, two moisture maxima are observed, one inside the averaging area near 115-120°E and the other centered to the east of the averaging area near 130-140°E. At the initial phase, the easterly winds lead to small dry advection north of the equator and small moist advection to the south, resulting in a weak positive moisture advection in the averaging area. At the mature phase, although the convergent wind leads to a dry advection south of the equator, the westerly wind brings moisture from the maximum center north of the equator and results in moistening. As a result, the horizontal advection is also weak (Fig. 9d). In BOTC, the moisture maximum is located east of the averaging area near 140°E. At the initial phase the zonal wind anomalies are weaker than those in CTRL, but the gradient of specific humidity and meridional wind anomalies are larger. Both the zonal and meridional wind anomalies result in positive moisture advection in the averaging area. At the mature phase, similar to ERA-I, there is strong convergent wind to the equator, which lead to strong dry advection. Note that the mean state of specific humidity and moisture gradients changed considerably from CTRL to BOTC. Compared with CTRL, the larger moisture gradients in BOTC along with anomalous wind result in the horizontal advection similar to that of ERA-I. Comparatively, the changes in moisture gradients contribute more to this improvement (not shown). This indicates that the altered mean state from modified parameterization may also have some effect on the MJO simulation besides convection organization itself (Jiang, 2017; Ahn et al., 2020).

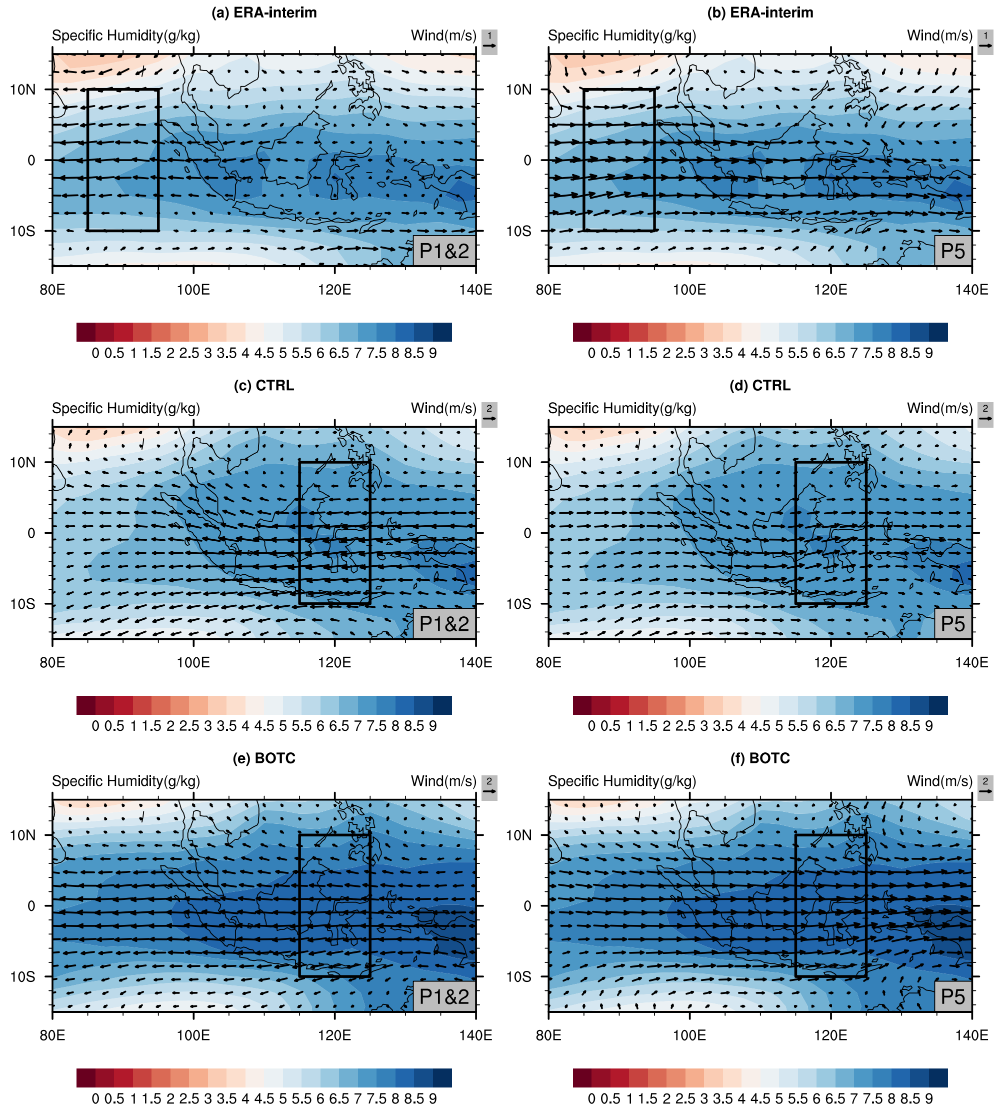

Fig. 9. Composites of 700 hPa anomalous horizontal winds (m/s) and mean specific humidity (g/kg) in MJO suppressed phases and mature phase in (a), (b) ERA-interim, (c), (d) CTRL, and (e), (f) BOTC. Here the mean specific humidity is multi-year averaged daily specific humidity over winter half of the year. The rectangles represent the averaging areas used in previous plots.

The column confined moisture tendency is a result of competing effects of dynamic and thermodynamic processes. For instance, cloud condensation depletes moisture, and therefore acts to impede the maintenance of moisture anomalies. However, condensational heating will result in upward motion, which moistens the atmosphere by transporting moisture-rich air from the low levels upward. The net effect can be either moistening or drying the atmospheric column, depending on the moisture and temperature stratification. By the same token, radiative cooling, although not directly affecting the moisture field, will result in sinking motion and thus dries the atmosphere through vertical advection. Therefore, examining the individual contribution to the column confined moisture tendency can provide useful insight into the roles they play in moisture variation during MJO evolution.

Fig. 10 shows the moisture tendency terms from the column processes in Eq. (12) in the MJO suppressed and mature phases. The terms containing α represent moistening (drying) caused indirectly by vertical advection induced by heating (cooling). In suppressed phases, in both CTRL and BOTC the major moistening factor in the lower troposphere is the combined effects of condensation and evaporation in the convection environment of the GCM grid box. As explained earlier in section 2, the vertical moisture advection from condensational heating supplies more moisture than needed by condensation, resulting in a net moistening. It was shown in CZ17 that shallow convection is increased in BOTC and there are positive low-level moisture and heating anomalies ahead of deep convection as MJO propagates eastward. Also, there are positive anomalies of vertical advection of moisture in the lower troposphere in advance of precipitation (Fig. 8 of CZ17). These together indicate that the low-level moistening from condensation anomalies is tightly associated with enhanced shallow convection. This is in agreement with CRM studies in Janiga and Zhang (2016). Note that while moistening from shallow convection ahead of deep convection in MJOs is well known, the interpretation may vary. On the one hand, evaporation from shallow convection in the convection environment can moisten the lower troposphere. On the other hand, under WTG approximation condensational heating will induce grid-scale upward motion, which will moisten the environment, although in the convection-free environment there can be compensating subsidence. Their combined effect is to moisten the atmosphere.

Consistent with the column MSE budget analysis, the radiative cooling leads to anomalous descent and dries most of the column, especially the lower troposphere. The drying tendencies are larger in BOTC than in CTRL. The moisture tendency due to freezing/melting from phase transition is positive near 600 hPa and negative above the height of 550 hPa. The moistening is due to less melting (compared to MJO lifecycle average) and the drying above is due to less freezing. The effects of detrainment and vertical diffusion are relatively small in the entire free troposphere, but quite large in the PBL in BOTC. In CTRL, the net column confined moisture tendency is positive from the surface to 450 hPa, which may contribute to fast development of convection. On the other hand, the positive net column confined moisture tendency in BOTC only extends to 600 hPa, with strong drying above. This may act to delay the development of deep convection. Thus, the important role of shallow convection in the MJO suppressed phases is further confirmed by examining the physical processes associated with vertical structure of moisture tendency variation.

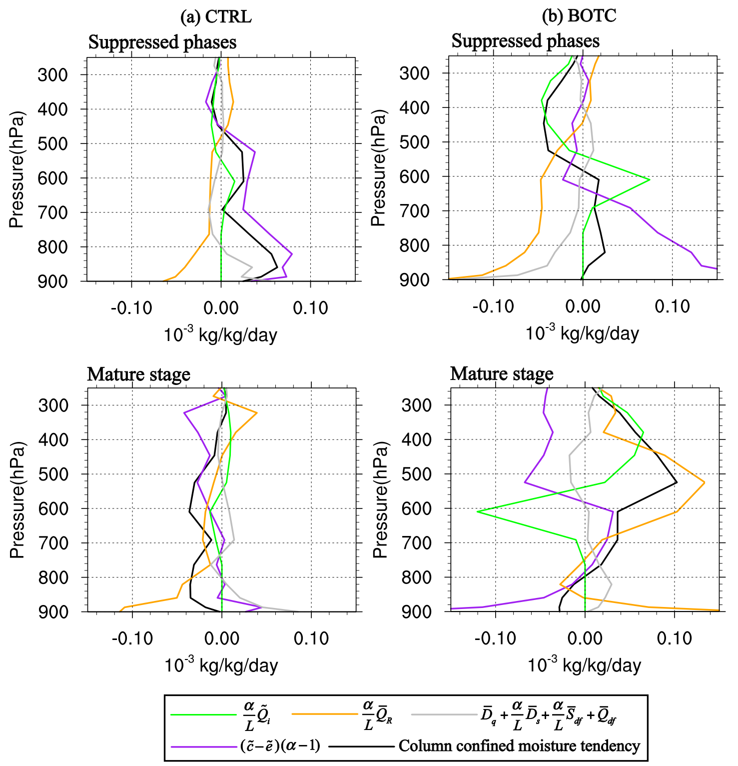

Fig. 10. Composite column confined moisture tendency and its components in Eq. (12) in suppressed (top row) and mature phase (bottom row), averaged over Maritime Continent (115-125°E,10°S-10°N) for (a) CTRL and (b) BOTC.

At the mature stage, the dominant contributor to the positive column confined moisture tendency in BOTC is radiative heating, which almost moistens the whole column and peaks at the midlevel. The decomposition into shortwave and longwave heating contributions separately (not shown) finds that longwave heating-induced moistening dominates throughout the troposphere below the 300 hPa height whereas the shortwave heating/cooling has a moistening effect in the upper troposphere and drying effect in the lower troposphere, with maximum drying near 800 hPa. The net large-scale condensation minus evaporation dries the upper troposphere and moistens the lower troposphere between 800 and 600 hPa. However, in the PBL there is strong drying, likely from evaporation-induced subsidence, which is largely balanced by radiative heating. We should point out that caution must be taken when interpreting the results in the PBL since the WTG approximation only holds in the free troposphere above the PBL. Because of the strong precipitation from higher levels associated with active deep convection, more ice/snow melting cools the midtroposphere near 600 hPa and thereby the induced subsidence substantially dries the layer. On the other hand, liquid freezing or ice/snow formation moistens the upper troposphere. In comparison with BOTC, CTRL shows entirely different vertical structure with the negative column confined moisture tendency at all levels below 400 hPa. Together with the vertical profile of column confined moisture tendency in suppressed phases and vertical structure of moisture in Fig. 6, it can be concluded that convection in CTRL develops too early and thus there is not enough active deep convection at the mature phase.

4. Discussion and Conclusions

Benefitting from a realistic simulation of MJO (the BOTC run) by modifying the vertical convective heating profile in the NCAR CAM5, this study examines contributions from different physical processes to moisture variations during different MJO phases, especially in the suppressed and mature phases. The objective is to understand what processes contribute the most to the MJO improvement, including its eastward propagation, in CAM5 simulation when the vertical heating profiles are modified to mimic the heating from mesoscale convective systems. The column MSE budget shows that in suppressed phases both horizontal and vertical advection contribute positively to MSE anomaly ahead of the MJO-associated deep convection. The vertical advection dominates the maintenance of vertically integrated MSE anomaly while radiative heating and surface fluxes act to reduce MSE in ERA-I and simulations. The opposite is true at the mature stage. However, they are largely balanced, leaving the horizontal advection governing the evolution of MSE tendency anomaly, leading to the eastward propagation of the MJO convection center. Although CTRL can produce these processes related to the column MSE budget, their magnitude is small and propagation is less organized, which result in large biases in MSE anomalies during MJO lifecycle. The analysis of column confined moisture tendency demonstrates the role of enhanced shallow convection (i.e., acting as an important source of low-level moisture in the suppressed phases of MJO) on the improved MJO simulation in BOTC. The moisture anomalies associated with shallow convection is due to vertical advection by the large-scale ascent induced by latent heat release from condensation rather than due to direct detrainment of moisture from shallow convection. This is because shallow convection drives a strong low-level moisture convergence through heating to force large-scale vertical upward motion (Wu, 2003) and in the lower troposphere below the level of minimum MSE vertical advection is more efficient in moistening the atmosphere than condensational depletion of moisture.

In the BOTC simulation, the horizontal advection of column MSE serves to increase (decrease) the MSE anomalies before (after) MJO develops to the mature phase. There is a shallow layer of positive MSE anomalies dominated by the horizontal advection in the lower troposphere ahead of MJO convection, helping the MJO to propagate eastward. The CTRL simulation fails to capture this feature. In the vertical structure of moisture budget, the net moisture tendency largely follows the anomalous horizontal advection in the whole column and peaks at mid-level in the MJO initial stages for ERA-I and BOTC. CTRL has small net moisture tendency with a maximum at lower troposphere during earlier phase, indicating too early convection. The column longwave radiative heating and latent heat flux have a positive correlation with precipitation anomalies, implying that these two terms maintain the column MSE during the enhanced MJO convection stages and help to stabilize the atmosphere during the initial stage, opposite to the vertical advection. The vertical profiles of column confined moisture tendency are examined with the aid of WTG approximation to help understand the contributions to the column moisture variation including the interaction between the cloud processes and vertical advection. It shows that the downward vertical advection induced by radiative cooling is essential to moisture budget in balancing the moistening from other processes in the initial stage, consistent with the column MSE budget analysis. At the mature phase, advective moistening from radiative heating-induced upward motion is a major source to maintain the moisture anomalies. The improvement in BOTC is attributed to the effects from increased shallow convection, which helps moisten the atmosphere below 600 hPa during suppressed phases and advance the eastward evolution afterwards.

As a follow up work of CZ17, this study provides a better understanding of the underlying mechanisms for the improved MJO simulation in BOTC from the view of moisture variations in MJO lifecycle. Based on the vertically integrated MSE budget and vertical profile of column confined moisture tendency analyses, this study confirms the physical mechanism of shallow convection in moistening the lower troposphere for the development of the deep convection during MJO evolution. It is also found that the role of vertical motion induced by radiative heating in moistening or drying is crucial to the MJO development. In a previous study, Wang and Sobel (2012) showed that radiative heating serves to destabilize the atmosphere when deep convection is enhanced in a CRM simulation. Wing and Emanuel (2014) suggested that radiative-convective feedbacks are important for the onset and organization of convection over tropics. Recent observations (Ciesielski et al., 2017) demonstrated that the radiative heating is essential in maintaining MJO during DYNAMO. In this study we showed that radiative heating and condensational heating in the convection environment are the two dominant terms in the column confined processes. These together with horizontal advection govern the moisture evolution in MJO.

Acknowledgments: This work is supported by the Science and Technology Project of Fujian Province under Grant Number 2023R1002006 and 2022R1002008. GJZ is supported by the U.S. National Science Foundation under grant AGS-2054697 and Department of Energy, Office of Science, Biological and Environmental Research Program (BER), under Award Numbers DE-SC0022064 and SC0023069. The authors would like to thank the three anonymous reviewers for their constructive comments that have helped improve the manuscript.

Availability Statement

The CAM5 simulation output for this study is available from a public data repository at Zenodo https://zenodo.org/records/10333148.

References

Adames, Á.F., 2017. Precipitation budget of the Madden–Julian oscillation. Journal of the Atmospheric Sciences 74, 1799–1817.

Adames, Á.F., Kim, D., 2016. The MJO as a dispersive, convectively coupled moisture wave: Theory and observations. Journal of the Atmospheric Sciences 73, 913–941.

Adames, Á.F., Maloney, E.D., 2021. Moisture Mode Theory's Contribution to Advances in our Understanding of the Madden-Julian Oscillation and Other Tropical Disturbances. Curr Clim Change Rep 7, 72–85. https://doi.org/10.1007/s40641-021-00172-4

Adames, Á.F., Wallace, J.M., 2015. Three-dimensional structure and evolution of the moisture field in the MJO. Journal of the Atmospheric Sciences 72, 3733–3754.

Ahn, M.-S., Kim, D., Kang, D., Lee, J., Sperber, K.R., Gleckler, P.J., Jiang, X., Ham, Y.-G., Kim, H., 2020. MJO propagation across the Maritime Continent: Are CMIP6 models better than CMIP5 models? Geophysical Research Letters 47, e2020GL087250.

Andersen, J.A., Kuang, Z., 2012. Moist static energy budget of MJO-like disturbances in the atmosphere of a zonally symmetric aquaplanet. Journal of Climate 25, 2782–2804.

Back, L.E., Bretherton, C.S., 2006. Geographic variability in the export of moist static energy and vertical motion profiles in the tropical Pacific. Geophysical research letters 33.

Benedict, J.J., Randall, D.A., 2011. Impacts of idealized air–sea coupling on Madden–Julian oscillation structure in the superparameterized CAM. Journal of the Atmospheric Sciences 68, 1990–2008.

Benedict, J.J., Randall, D.A., 2007. Observed characteristics of the MJO relative to maximum rainfall. Journal of the atmospheric sciences 64, 2332–2354.

Bretherton, C.S., Park, S., 2009. A new moist turbulence parameterization in the Community Atmosphere Model. Journal of Climate 22, 3422–3448.

Cai, Q., Zhang, G.J., Zhou, T., 2013. Impacts of shallow convection on MJO simulation: A moist static energy and moisture budget analysis. Journal of Climate 26, 2417–2431.

Cao, G., Zhang, G.J., 2017. Role of vertical structure of convective heating in MJO simulation in NCAR CAM5. 3. Journal of Climate 30, 7423–7439.

Chen, C.-C., Richter, J.H., Liu, C., Moncrieff, M.W., Tang, Q., Lin, W., Xie, S., Rasch, P.J., 2021. Effects of organized convection parameterization on the MJO and precipitation in E3SMv1. Part I: Mesoscale heating. Journal of Advances in Modeling Earth Systems 13, e2020MS002401.

Chikira, M., 2014. Eastward-propagating intraseasonal oscillation represented by Chikira–Sugiyama cumulus parameterization. Part II: Understanding moisture variation under weak temperature gradient balance. Journal of the Atmospheric Sciences 71, 615–639.

Ciesielski, P.E., Johnson, R.H., Jiang, X., Zhang, Y., Xie, S., 2017. Relationships between radiation, clouds, and convection during DYNAMO. Journal of Geophysical Research: Atmospheres 122, 2529–2548.

DeMott, C.A., Klingaman, N.P., Woolnough, S.J., 2015. Atmosphere-ocean coupled processes in the Madden-Julian oscillation. Reviews of Geophysics 53, 1099–1154.

Derbyshire, S.H., Beau, I., Bechtold, P., Grandpeix, J.-Y., Piriou, J.-M., Redelsperger, J.-L., Soares, P.M.M., 2004. Sensitivity of moist convection to environmental humidity. Quarterly Journal of the Royal Meteorological Society: A journal of the atmospheric sciences, applied meteorology and physical oceanography 130, 3055–3079.

Grabowski, W.W., 2003. MJO-like coherent structures: Sensitivity simulations using the cloud-resolving convection parameterization (CRCP). Journal of the Atmospheric Sciences 60, 847–864.

Hannah, W.M., Maloney, E.D., 2011. The role of moisture–convection feedbacks in simulating the Madden–Julian oscillation. Journal of Climate 24, 2754–2770.

Hsu, P., Li, T., 2012. Role of the boundary layer moisture asymmetry in causing the eastward propagation of the Madden–Julian oscillation. Journal of Climate 25, 4914–4931.

Hsu, P.-C., Li, T., Murakami, H., 2014. Moisture asymmetry and MJO eastward propagation in an aquaplanet general circulation model. Journal of Climate 27, 8747–8760.

Huffman, G.J., Adler, R.F., Morrissey, M.M., Bolvin, D.T., Curtis, S., Joyce, R., McGavock, B., Susskind, J., 2001. Global precipitation at one-degree daily resolution from multisatellite observations. Journal of hydrometeorology 2, 36–50.

Huffman, G.J., Bolvin, D.T., Nelkin, E.J., Wolff, D.B., Adler, R.F., Gu, G., Hong, Y., Bowman, K.P., Stocker, E.F., 2007. The TRMM multisatellite precipitation analysis (TMPA): Quasi-global, multiyear, combined-sensor precipitation estimates at fine scales. Journal of hydrometeorology 8, 38–55.

Hung, M.-P., Lin, J.-L., Wang, W., Kim, D., Shinoda, T., Weaver, S.J., 2013. MJO and convectively coupled equatorial waves simulated by CMIP5 climate models. Journal of Climate 26, 6185–6214.

Janiga, M.A., Zhang, C., 2016. MJO moisture budget during DYNAMO in a cloud-resolving model. Journal of the Atmospheric Sciences 73, 2257–2278.

Jiang, X., 2017. Key processes for the eastward propagation of the Madden-Julian Oscillation based on multimodel simulations. Journal of Geophysical Research: Atmospheres 122, 755–770. https://doi.org/10.1002/2016JD025955

Kim, D., Kim, H., Lee, M.-I., 2017. Why does the MJO detour the Maritime Continent during austral summer? Geophysical Research Letters 44, 2579–2587. https://doi.org/10.1002/2017GL072643

Kim, D., Xavier, P., Maloney, E., Wheeler, M., Waliser, D., Sperber, K., Hendon, H., Zhang, C., Neale, R., Hwang, Y.-T., 2014. Process-oriented MJO simulation diagnostic: Moisture sensitivity of simulated convection. Journal of Climate 27, 5379–5395.

Kiranmayi, L., Maloney, E.D., 2011. Intraseasonal moist static energy budget in reanalysis data. Journal of Geophysical Research: Atmospheres 116.

Le, P.V., Guilloteau, C., Mamalakis, A., Foufoula-Georgiou, E., 2021. Underestimated MJO variability in CMIP6 models. Geophysical research letters 48, e2020GL092244.

Li, T., 2014. Recent advance in understanding the dynamics of the Madden-Julian oscillation. Journal of Meteorological Research 28, 1–33.

Li, T., Ling, J., Hsu, P.-C., 2020. Madden-Julian oscillation: Its discovery, dynamics, and impact on East Asia. Journal of Meteorological Research 34, 20–42.

Liu, F., Wang, B., 2016. Role of Horizontal Advection of Seasonal-Mean Moisture in the Madden–Julian Oscillation: A Theoretical Model Analysis. https://doi.org/10.1175/JCLI-D-16-0078.1

Liu, Y., Tan, Z.-M., Wu, Z., 2022. Enhanced feedback between shallow convection and low-level moisture convergence leads to improved simulation of MJO eastward propagation. Journal of Climate 35, 591–615.

Madden, R.A., Julian, P.R., 1972. Description of global-scale circulation cells in the tropics with a 40–50 day period. Journal of Atmospheric Sciences 29, 1109–1123.

Madden, R.A., Julian, P.R., 1971. Detection of a 40–50 day oscillation in the zonal wind in the tropical Pacific. Journal of Atmospheric Sciences 28, 702–708.

Maloney, E.D., 2009. The moist static energy budget of a composite tropical intraseasonal oscillation in a climate model. Journal of Climate 22, 711–729.

Maloney, E.D., Sobel, A.H., Hannah, W.M., 2010. Intraseasonal variability in an aquaplanet general circulation model. Journal of Advances in Modeling Earth Systems 2.

Mapes, B.E., 2000. Convective inhibition, subgrid-scale triggering energy, and stratiform instability in a toy tropical wave model. Journal of the Atmospheric Sciences 57, 1515–1535.

Mayta, V.C., Adames Corraliza, Á.F., 2023. Is the Madden-Julian Oscillation a Moisture Mode? Geophysical Research Letters 50, e2023GL103002. https://doi.org/10.1029/2023GL103002

Mu, M., Zhang, G.J., 2008. Energetics of Madden Julian oscillations in the NCAR CAM3: A composite view. Journal of Geophysical Research: Atmospheres 113.

Neale, R.B., Chen, C.-C., Gettelman, A., Lauritzen, P.H., Park, S., Williamson, D.L., Conley, A.J., Garcia, R., Kinnison, D., Lamarque, J.-F., 2010. Description of the NCAR community atmosphere model (CAM 5.0). NCAR Tech. Note NCAR/TN-486+ STR 1, 1–12.

Neelin, J.D., Held, I.M., 1987. Modeling tropical convergence based on the moist static energy budget. Monthly Weather Review 115, 3–12.

Park, S., Bretherton, C.S., 2009. The University of Washington shallow convection and moist turbulence schemes and their impact on climate simulations with the Community Atmosphere Model. Journal of Climate 22, 3449–3469.

Raymond, D.J., Sessions, S.L., Sobel, A.H., Fuchs, Ž., 2009. The mechanics of gross moist stability. Journal of Advances in Modeling Earth Systems 1.

Sherwood, S.C., 1999. Convective precursors and predictability in the tropical western Pacific. Monthly Weather Review 127, 2977–2991.

Shin, J., Baik, J.-J., 2023. Global simulation of the Madden–Julian oscillation with stochastic unified convection scheme. Journal of Advances in Modeling Earth Systems 15, e2022MS003578.

Simmons, A., Uppala, S., Dee, D., Kobayashi, S., 2007. ERA-Interim: New ECMWF reanalysis products from 1989 onwards. https://doi.org/10.21957/POCNEX23C6

Slingo, J., Inness, P., Neale, R., Woolnough, S., Yang, G., 2003. Scale interactions on diurnal toseasonal timescales and their relevanceto model systematic errors. Annals of Geophysics.

Sobel, A., Maloney, E., 2013. Moisture modes and the eastward propagation of the MJO. Journal of the Atmospheric Sciences 70, 187–192.

Sobel, A.H., Nilsson, J., Polvani, L.M., 2001. The weak temperature gradient approximation and balanced tropical moisture waves. Journal of the atmospheric sciences 58, 3650–3665.

Wang, B., Lee, S.-S., Waliser, D.E., Zhang, C., Sobel, A., Maloney, E., Li, T., Jiang, X., Ha, K.-J., 2018. Dynamics-oriented diagnostics for the Madden–Julian Oscillation. Journal of Climate 31, 3117–3135.

Wang, L., Li, T., 2020. Reexamining the MJO moisture mode theories with normalized phase evolutions. Journal of Climate 33, 8523–8536.

Wang, L., Li, T., Maloney, E., Wang, B., 2017. Fundamental causes of propagating and nonpropagating MJOs in MJOTF/GASS models. Journal of Climate 30, 3743–3769.

Wang, S., Sobel, A.H., 2012. Impact of imposed drying on deep convection in a cloud-resolving model. Journal of Geophysical Research: Atmospheres 117.

Wheeler, M.C., Hendon, H.H., 2004. An all-season real-time multivariate MJO index: Development of an index for monitoring and prediction. Monthly weather review 132, 1917–1932.

Wing, A.A., Emanuel, K.A., 2014. Physical mechanisms controlling self-aggregation of convection in idealized numerical modeling simulations. Journal of Advances in Modeling Earth Systems 6, 59–74.

Wolding, B.O., Maloney, E.D., 2015. Objective diagnostics and the Madden–Julian oscillation. Part II: Application to moist static energy and moisture budgets. Journal of Climate 28, 7786–7808.

Wolding, B.O., Maloney, E.D., Branson, M., 2016. Vertically resolved weak temperature gradient analysis of the M adden-J ulian O scillation in SP-CESM. Journal of Advances in Modeling Earth Systems 8, 1586–1619.

Wu, Z., 2003. A shallow CISK, deep equilibrium mechanism for the interaction between large-scale convection and large-scale circulations in the tropics. Journal of the atmospheric sciences 60, 377–392.

Yanai, M., Esbensen, S., Chu, J.-H., 1973. Determination of bulk properties of tropical cloud clusters from large-scale heat and moisture budgets. Journal of Atmospheric Sciences 30, 611–627.

Zhang, C., 2013. Madden–Julian oscillation: Bridging weather and climate. Bulletin of the American Meteorological Society 94, 1849–1870.

Zhang, C., 2005. Madden-julian oscillation. Reviews of Geophysics 43.

Zhang, C., Adames, Á.F., Khouider, B., Wang, B., Yang, D., 2020. Four Theories of the Madden-Julian Oscillation. Reviews of Geophysics 58, e2019RG000685. https://doi.org/10.1029/2019RG000685

Zhang, G.J., McFarlane, N.A., 1995. Sensitivity of climate simulations to the parameterization of cumulus convection in the Canadian climate centre general circulation model. Atmosphere Ocean 33, 407–446.

Zhang, G.J., Mu, M., 2005. Effects of modifications to the Zhang-McFarlane convection parameterization on the simulation of the tropical precipitation in the National Center for Atmospheric Research Community Climate Model, version 3. Journal of Geophysical Research: Atmospheres 110.

Zhang, G.J., Song, X., 2009. Interaction of deep and shallow convection is key to Madden-Julian Oscillation simulation. Geophysical Research Letters 36.